Preparation of Neptunyl and Plutonyl Acetates to Access Non-Aqueous Transuranium Coordination Chemistry

Emily R. Mikeska,[†,‡] Richard E. Wilson,[*,‡] Asmita Sen,[¶] Jochen Autschbach,[*,¶] and James D. Blakemore[*,†]

†Department of Chemistry, University of Kansas, 1567 Irving Hill Road, Lawrence, KS 66045

‡Chemical Sciences and Engineering Division, Argonne National Laboratory, Lemont, IL 60439

¶Department of Chemistry, University of Buffalo, State University of New York. Natural Sciences Complex, Buffalo, NY, 14260

E-mail: rewilson@anl.gov; jochena@buffalo.edu; blakemore@ku.edu

Abstract

Uranyl diacetate dihydrate is a useful reagent for the preparation of uranyl (UO_2^{2+}) coordination complexes, as it is a well-defined stoichiometric compound featuring moderately basic acetates that can facilitate protonolysis reactivity, unlike other anions commonly used in synthetic actinide chemistry such as halides or nitrate. Despite these attractive features, analogous neptunium (Np) and plutonium (Pu) compounds are unknown to date. Here, a modular synthetic route is reported for accessing stoichiometric neptunyl(VI) and plutonyl(VI) diacetate compounds that can serve as starting materials for transuranic coordination chemistry. The new NpO_2^{2+} and PuO_2^{2+}

1

complexes, as well as a corresponding molecular UO_2^{2+} complex, are isomorphous in the solid state, and in solution show similar solubility properties that facilitate their use in synthesis. In both solid and solution state, the +VI oxidation state (O.S.) is maintained, as demonstrated by vibrational and optical spectroscopy, confirming that acetate anions can stabilize the oxidizing, high-valent +VI states of Np and Pu as they do for the relatively more stable U(VI). All three acetate salts react smoothly with a model diprotic ligand, affording incorporation of U(VI), Np(VI), and Pu(VI) cores into molecular coordination compounds that occurs concomitantly with elimination of acetic acid; the new complexes are high-valent, yet overall charge neutral, facilitating entry into non-aqueous chemistry by rational synthesis. Joint computational studies reveal that the dianionic ligand framework assists in stabilizing the +VI O.S. through strong sigma donation to the 5f shells of the actinides, highlighting the potential usefulness of protonolysis reactivity toward preparation of stabilized high-valent transuranic species.

Introduction

Protonolysis reactivity is a classic strategy for the preparation of metal coordination complexes. Protonolysis involves proton (H^+) transfer from incoming ligands (often organic in nature) to outgoing (often inorganic) ligands found in starting materials, avoiding both the need for an exogeneous base and/or the co-generation of salts that can complicate isolation of the desired product. Metal acetate salts are one attractive class of compounds that are useful for protonolysis reactivity, as they generate equivalents of acetic acid (a volatile species readily removed *in vacuo*) upon treatment with suitable protic ligand precursors. Many metal acetates are commercially available, including uranyl acetate, $UO_2(CH_3COO)_2H_2O \cdot H_2O$, and protonolysis reactivity has been documented across most areas of the periodic table.[1–4] However, protonolysis reactivity represents a synthetic strategy that has received less attention than it deserves in the realm of transuranic chemistry, particularly the chemistry of neptunium (Np) and plutonium (Pu).

https://doi.org/10.26434/chemrxiv-2024-kqthl-v2 **ORCID:** https://orcid.org/0000-0003-4172-7460 Content not peer-reviewed by ChemRxiv. **License:** CC BY-NC-ND 4.0

Generally speaking, the paucity of discrete, well-characterized starting materials has hindered advancements in the chemistry of Np and Pu.[5–7] Although the radioactivity of Np and Pu limits the facilities in which they can be handled, investigation of these not naturally occurring elements is an outstanding challenge in both actinide and sustainability science, owing to their presence in the fuel cycle for low-carbon nuclear energy. Progress in the field has been more brisk in recent years with renewed focus placed on the identification of starting materials. Notable among these, solvent adducts of the actinide chlorides such as $AnI_3(THF)_3$, $An(N(SiCH_3)_2)_3$ and $AnCl_4(DME)_2$ (An = U, Np, Pu) have been reported and successfully used for preparation of low-valent complexes.[5,8,9] However, fewer well-defined starting materials are known for the high-valent oxidation states that are also compatible with non-aqueous conditions. Two commonly employed compounds of this type are $[Ph_4P]_2[AnO_2Cl_4]$ (An = Np and Pu)[10] and $[NpO_2Py_5][KI_2Py_2]_2$ (see Figure 1).[11] Additionally, "putative" materials obtained by isolation of solids from sensible solution conditions can be utilized quite effectively,[12] despite the limited characterization sometimes available for these species.

In any case, the identity of the anion that accompanies a metal, transuranic or otherwise, dictates the feasibility of protonolysis reactivity and other reactivity pathways. Halides (and nitrate) are nearly always not intrinsically basic enough, in the Brønsted-Lowry sense, to enable facile proton abstraction from incoming organic ligands, curtailing synthetically useful protonolysis reactivity. Considering this, we anticipated that pursuit of $NpO_2{}^{2+}$ and $PuO_2{}^{2+}$ diacetate complexes could afford a new class of starting materials useful for protonolysis that could, in turn, be used to generate coordination complexes featuring actinyl motifs. Such an approach has the potential to open new synthetic opportunities that avoid difficulties encountered in other approaches. However, care is needed to avoid formation of the well-known tris(acetato) salts of the actinyls $AnO_2{}^{2+}$ (An = U, Np, Pu) with alkali metal co-cations.[13,14] These compounds have been documented as very insoluble in most media, a finding exploited in a separations method for actinyl ions relying on fractional crystallization.[15] We were mo-
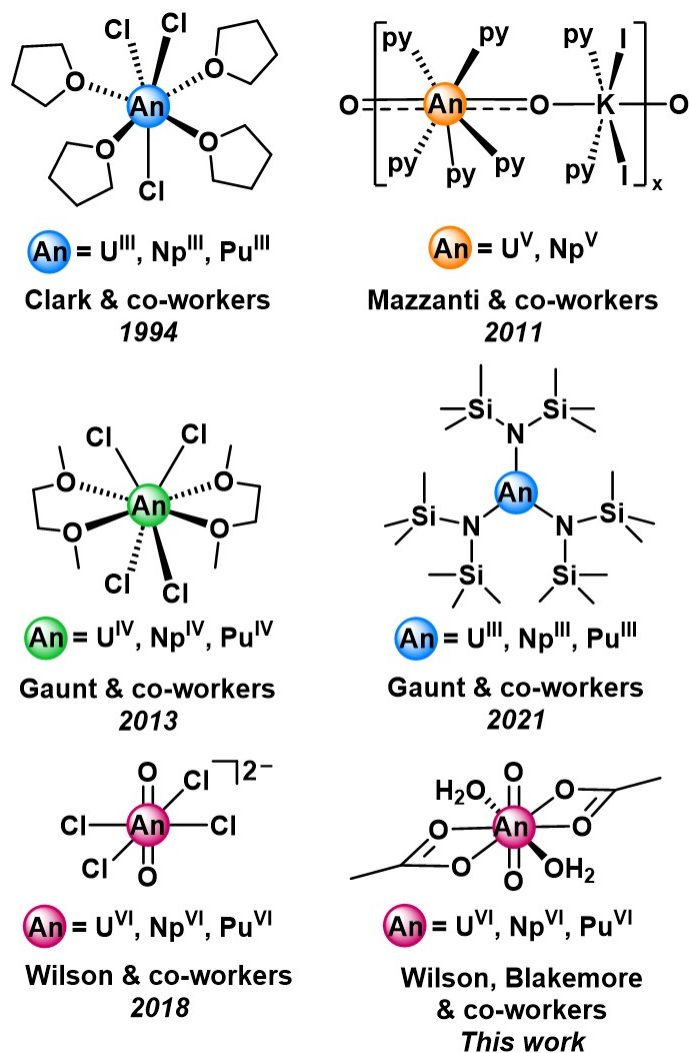
3

Figure 1: Examples of well-defined actinide starting materials.

tivated here by the enduring utility of $UO_2(CH_3COO)_2H_2O \cdot H_2O$, which is neutral and offers a synthetically useful degree of solubility in polar solvents. As the actinyl dications have similar effective metal charges (as estimated through solvent extraction and potentiometric titration experiments) of $+3.2$ for U(VI), $+3.0$ for Np(VI) and $+2.9$ for Pu(VI),[16] we anticipated that Np- and Pu-based analogues of uranyl acetate might be stable and isolable as well, envisioning that the resulting complexes could be useful as starting materials for transuranic coordination chemistry.

Here, we report the synthesis, structural, and spectroscopic characterization of $UO_2{}^{2+}$, $NpO_2{}^{2+}$, and $PuO_2{}^{2+}$ diacetates, and their use as starting materials for non-aqueous transuranic coordination chemistry. The starting materials are prepared by ozonolysis of $U(OH)_4(H_2O)_x$, $Np(OH)_4(H_2O)_x$, and $Pu(OH)_4(H_2O)_x$ in acetic acid forming $AnO_2(CH_3COO)_2(H_2O)_2 \cdot CH_3COOH$ (An = U, Np and Pu). Virtually complete avoidance of the noted triacetato species was achieved through use of the tetrahydroxide materials in our synthetic route, as they are non-amphoteric and can be obtained by precipitation from concentrated NaOH without retention of sodium cations. The utility of the reported Np(VI) and Pu(VI) diacetates as starting materials for coordination chemistry is demonstrated through the reaction of these compounds with a diprotic Schiff base forming coordination complexes that retain the +VI O.S. of both Np and Pu, thus forming a homologous series. Structural, spectroscopic, and computational characterization of the series is presented, highlighting trends in the chemical reactivity across the early actinides U, Np, and Pu.

Results

Synthesis of $AnO_2(CH_3COO)_2(H_2O)_2 \cdot CH_3COOH$ (An = U, Np, and Pu)

Commercially available uranyl diacetate dihydrate exists as a coordination polymer prepared by evaporation of an acetic acid solution of $UO_2{}^{2+}$.[17] A monomeric phase of uranyl acetate

5

https://doi.org/10.26434/chemrxiv-2024-kqthl-v2 **ORCID:** https://orcid.org/0000-0003-4172-7460 Content not peer-reviewed by ChemRxiv. **License:** CC BY-NC-ND 4.0

containing two co-crystallized acetic acid molecules has been previously reported, as well as an anhydrous polymeric phase, both of which are prepared by crystallization from glacial acetic acid.[18,19] In this work, we chose to prepare neptunyl and plutonyl acetate species through the oxidation of Np(IV) or Pu(IV) by ozonolysis in glacial acetic acid as shown in Figure 2; the isostructural uranium compound was prepared in the same manner using oxygen instead of ozone as the oxidant. Direct ozonolysis of acetic acid solutions containing the transuranic ions of interest proved to be an effective route to accessing the diacetate salts because of the resistance of acetic acid to oxidation by ozone and because of the stabilization of ozone by acetic acid. Prior work has shown these attractive features are due, at least in part, to the ability of CH_3COOH to scavenge radical species that would facilitate the decomposition of ozone.[20,21]

$$An(OH)_4 + CH_3COOH \xrightarrow{O_2/O_3} AnO_2(CH_3COO)_2(H_2O)_2 \cdot CH_3COOH$$

Figure 2: Synthetic scheme for accessing $AnO_2(CH_3COO)_2(H_2O)_2 \cdot CH_3COOH$ (An = U, Np, and Pu) by direct oxidation with oxygen or ozone.

Initial synthetic attempts to prepare the Np(VI) and Pu(VI) acetates by the direct precipitation of An(VI) from mineral acid solutions with strong base (e.g., NaOH) resulted in the formation of $NaNpO_2(CH_3COO)_3$ and $NaPuO_2(CH_3COO)_3$ when even small amounts of sodium ion were present in the actinide hydroxide precipitate. This behavior is in accord with prior reports of formation of ternary neptunyl and plutonyl hydroxide phases which can result if complete reduction to the +IV state is not achieved (e.g. $M[AnO_2(OH)_2]$ where M = Na, K, Rb, Cs and An = Np, Pu),[22–25] when mineral acid solutions are treated with alkali metal hydroxides to precipitate An(V) and An(VI). These actinyl materials carry the alkali metal ions through the reaction sequence, resulting in the formation of $NaAnO_2(CH_3COO)_3$ phases. We also considered implementing cation exchange chromatography in our work here, but ultimately did not pursue this because of the reported reduction of Np and Pu on cation exchange columns to the tetravalent state coupled with the high affinity of An(IV) ions for

6

the resins.[26,27]

Considering all this, we noted at the start of our investigations that the An(IV) hydroxides do not form ternary phases with alkali metals, are highly insoluble, and easily prepared by chemical or electrochemical reduction of the actinides in mineral acids. The needed An(IV) hydroxides were thus prepared by precipitation with NaOH from a mineral (typically, nitric) acid solution of the actinide in the +IV oxidation state and washed thoroughly with water to eliminate residual sodium ions. The negligible solubility of An(IV) hydroxides resulted in near quantitative precipitation, in accord with literature reports.[26,28] Oxidation of $An(OH)_4(H_2O)_x$ (An = Np or Pu) in acetic acid by ozone and subsequent work-up afforded high yields of single crystals with the formulation $AnO_2(CH_3COO)_2(H_2O)_2 \cdot CH_3COOH$ (denoted **NpOAc** and **PuOAc**).

The reaction conditions useful for Np and Pu in the synthesis vary slightly, as one could anticipate based on the intrinsic acidity differences between the various oxidation states of the elements. Ozonolysis of $Np(OH)_4(H_2O)_x$ in acetic acid and concentration of that solution by gentle heating first results in the formation of a green precipitate likely corresponding to a monoacetate species of Np(V).[29] Indeed, vibrational spectra collected on this green material compare well to those of $NpO_2CH_3COO \cdot H_2O$ as reported by Bessonov and co-workers (see SI, Figures S5, S6, and S22). This intermediate is the solubility limiting phase in glacial acetic acid, but continued ozonolysis of the material in glacial acetic acid with stirring produces solid magenta **NpOAc** in high yield (80%). Over multiple preparations of this material, we have identified that the reaction yield is sensitive to both the concentration of neptunium in the reaction mixture and the concentration of acetic acid present (both must be as high as possible for best results). Additionally, a polymeric phase of Np(VI) that is isostructural to the commercially available $UO_2(CH_3COO)_2H_2O \cdot H_2O$ was isolated on one occasion by rapidly cooling a solution of Np(VI) in glacial acetic acid (see SI, pp. 87-90 and Table ST8 for details on this structure).

In the case of plutonium, the reaction proceeds at a slower rate than for neptunium,

7

requiring several days to form the target Pu(VI) diacetate compound. This could be a consequence of the enhanced thermodynamic stability of Pu(IV) compared to Np(IV).[26,27] However, similar to the case of neptunium, we found the plutonium reaction to be sensitive to concentration with an optimal concentration of approx. 10 mg/mL of plutonium in glacial CH_3COOH. Preparation of the Pu(VI) diacetate compound does not result in precipitation of an intermediate Pu(V)-acetate species as was the case for neptunium; such a species is likely precluded by the established instability of Pu(V) in acidic media.[27]

In order to put forth a comprehensive view of the behavior of molecular actinyl species in the diacetate system, we also prepared the corresponding uranyl diacetate by applying our strategy to the $U(OH)_4(H_2O)_x$ starting material. Although synthesis of **NpOAc** and **PuOAc** require ozone as the oxidant ($E°(O_3/O_2) = +2.07$ V vs. the standard hydrogen electrode, SHE), simply bubbling air through a slurry of $U(OH)_4(H_2O)_x$ in glacial acid overnight yielded uranyl diacetate species.[30] This is consistent with the greater stability of $UO_2{}^{2+}$ compared to $NpO_2{}^{2+}$ and $PuO_2{}^{2+}$ such that O_2 is sufficiently oxidizing to push the reaction forward ($E°(O_2/H_2O) = +1.23$ V vs. SHE).[30] These conditions could be used to prepare either a triclinic molecular uranyl diacetate phase (**UOAc-No2**; see SI, pp. 84-87 and Table ST8) for details on this structure) or a monoclinic molecular uranyl diacetate, denoted **UOAc**, which is isomorphous with **NpOAc** and **PuOAc**.

Structures of $AnO_2(CH_3COO)_2(H_2O)_2 \cdot CH_3COOH$ (An = U, Np, and Pu)

Magenta prisms harvested from the synthesis of **NpOAc** and green plates harvested from the analogous preparation of **PuOAc** were studied using single crystal X-ray diffraction (XRD) analysis. The structures reveal isostructural compounds of the formulation $AnO_2(CH_3COO)_2$ $(H_2O)_2 \cdot CH_3COOH$ (An = Np and Pu) that crystallized in the centrosymmetric space group $C2/c$ as shown in Figure 3.

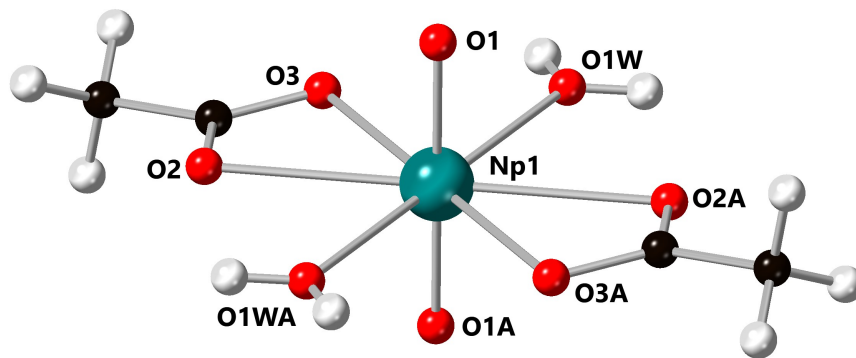The solution and refinement of the structures of **UOAc**, **NpOAc**, and **PuOAc** all pro-

8

Figure 3: Ball and stick representation of the solid-state structure of **NpOAc** as a representative structure for the isomorphous **UOAc**, **NpOAc**, and **PuOAc** series. A co-crystallized acetic acid molecule is omitted for clarity.

ceeded in a straightforward manner. Details regarding the crystallography are provided in the Supporting Information (pp. 75-83 and Table ST7), with the structural details for each of the complexes given in Table 1. In each case, the actinyl diacetate species is molecular in nature in the solid state. Only hydrogen bonding interactions hold the species together in the solid state, and there are no ligands bridging between metal centers. The actinide atoms are situated on inversion centers in the asymmetric units of the structures; as a result, the isostructural **UOAc**, **NpOAc**, and **PuOAc** display C_{2h} site symmetry from the perspective of the nonhydrogen atoms in the structures.

All three structures feature virtually linear actinyl moieties, with actinide centers coordinated to two κ^2-acetates and two water molecules in the equatorial plane. An additional co-crystallized acetic acid molecule is present in the lattice of each structure, engaging in hydrogen bonding with one bound acetate and one bound water. Each An-O_{yl} bond distance falls within the range typical for actinyl(VI) ions; a contraction from U (1.760(1) Å) to Np (1.748(1) Å) to Pu (1.740(3) Å) is observed, consistent with the ionic radii across the series.[31–33] The contraction noted in the actinyl bonds is not observed in the bond distances in the equatorial planes of **UOAc**, **NpOAc**, and **PuOAc**, with all three actinides possessing virtually identical An–$O_{acetate}$ bond distances. The lack of a contraction in the equatorial bond distances from U to Pu has been observed in studies of series of

9

[AnO$_2$] complexes including the halides and nitrates,[34] a phenomenon attributable to diminished in-plane covalency. The equatorial bond distances observed in the polymeric phase UO$_2$(CH$_3$COO)$_2$H$_2$O·H$_2$O show shorter bonds between the carboxylate oxygen atoms and U compared to the molecular phase, likely a result of the lower coordination number and less steric hindrance about the U center in this phase (C.N. = 5) versus in the molecular phase of **UOAc**.

Table 1: Comparison of selected structural parameters from X-ray diffraction analyses of **UOAc**, **NpOAc**, and **PuOAc**.

	UOAc (Å)	**NpOAc** (Å)	**PuOAc** (Å)
An-O1	1.760(1)	1.748(1)	1.740(3)
An-O2	2.514(1)	2.516(1)	2.515(3)
An-O3	2.496(1)	2.496(2)	2.492(3)
An-O1W	2.446(1)	2.439(2)	2.438(3)

Vibrational and Optical Spectroscopy

Vibrational spectra of the actinyl(VI) diacetate compounds were collected in the solid state and are shown in Figure 4 (see SI, Figures S1-S4, S7, S8, S18-S21, S23, and S24 for full spectra). A summary of the key spectral features is also provided in Table 2. For an actinyl moiety on an inversion center in a centrosymmetric crystalline lattice, three vibrationally active normal modes, the Raman active symmetric stretch, ν_1, an IR active bending mode, ν_2, and an IR active asymmetric stretch, ν_3, may be observed and are mutually exclusive. In all cases, the symmetric stretches of the actinyl ions appear prominently in the Raman spectra at 870, 846, and 827 cm^{-1} for U, Np, and Pu, respectively, and are in the conventional range for the +VI oxidation state. Progressing from U to Np to Pu, a redshift of 43 cm^{-1} is observed, although the An≡O bond contracts across this series; this is similar to trends previously observed in other isostructural series of actinyl complexes and is likely derived from a decrease in overlap between the oxygen and actinide $5f$ orbitals as the actinides contract from U to Pu.[34–37] Two features associated with symmetric stretching of the O-C-

O moiety of the acetates can be observed at ca. 890 and 955 cm^{-1}, corresponding to the co-crystallized acetic acid found in the lattice and bound acetate, respectively (see SI, Table ST1 for a full assignment of the spectral features).[38,39]

Table 2: Comparison of selected Raman and IR frequencies (cm^{-1}) for **UOAc**, **NpOAc**, and **PuOAc**.

	UOAc	NpOAc	PuOAc
$\nu(AnO_2{}^{2+})_{sym}$	870	846	827
$\nu(AnO_2{}^{2+})_{asym}$	928	933	941
ν(C-O-C)*	893	892	892
ν(C-O-C)	955	953	954

*corresponds to co-crystallized acetic acid

Solid-state infrared spectra were also collected for each compound and revealed similar frequencies for the asymmetric v$_3$ stretches of the actinyl ions between 928 and 941 cm^{-1} for U, Np, and Pu. While uranyl diacetate dihydrate is a notably stable and very weakly oxidizing species, **NpOAc** displayed reactivity with KBr, the media used for preparing a sample of the compound for IR analysis. Comparison of IR spectra for **NpOAc** collected on two consecutive days revealed very similar spectra, with the exception of a prominent feature at 752 cm^{-1} in the spectrum on day two (see SI, Figures S18 - S21). This strong absorption resembles the asymmetric stretch of $NpO_2(CH_3COO)\cdot H_2O$, which has been reported at 772 cm^{-1} and which we measured at 752 cm^{-1} (see SI, Figure S22).[29] The formation of the Np(V) material over time is attributable to oxidation of bromide ($E°(Br_2/Br^-) = +1.07$ V) by **NpOAc**, in line with the value for $E°(Np^{VI}/Np^V)$ of $+1.14$ V.[26,40] KCl was employed as the matrix for the IR spectrum of **PuOAc**, and no formation of lower-valent material was observable in the resulting spectra.

Optical spectra of solutions of **UOAc**, **NpOAc**, and **PuOAc** in glacial acetic acid are presented in Figure 5 (see SI, Figure S31 - S36 for full spectra and molar absorptivity determinations). A vibronic progression can be seen at 417 nm in the spectrum of **UOAc**, resulting from the coupling of vibrational excited states to the ligand-to-metal-charge transfer (LMCT) transition from the oxo groups to U(VI).[41] Two prominent features at 564 nm
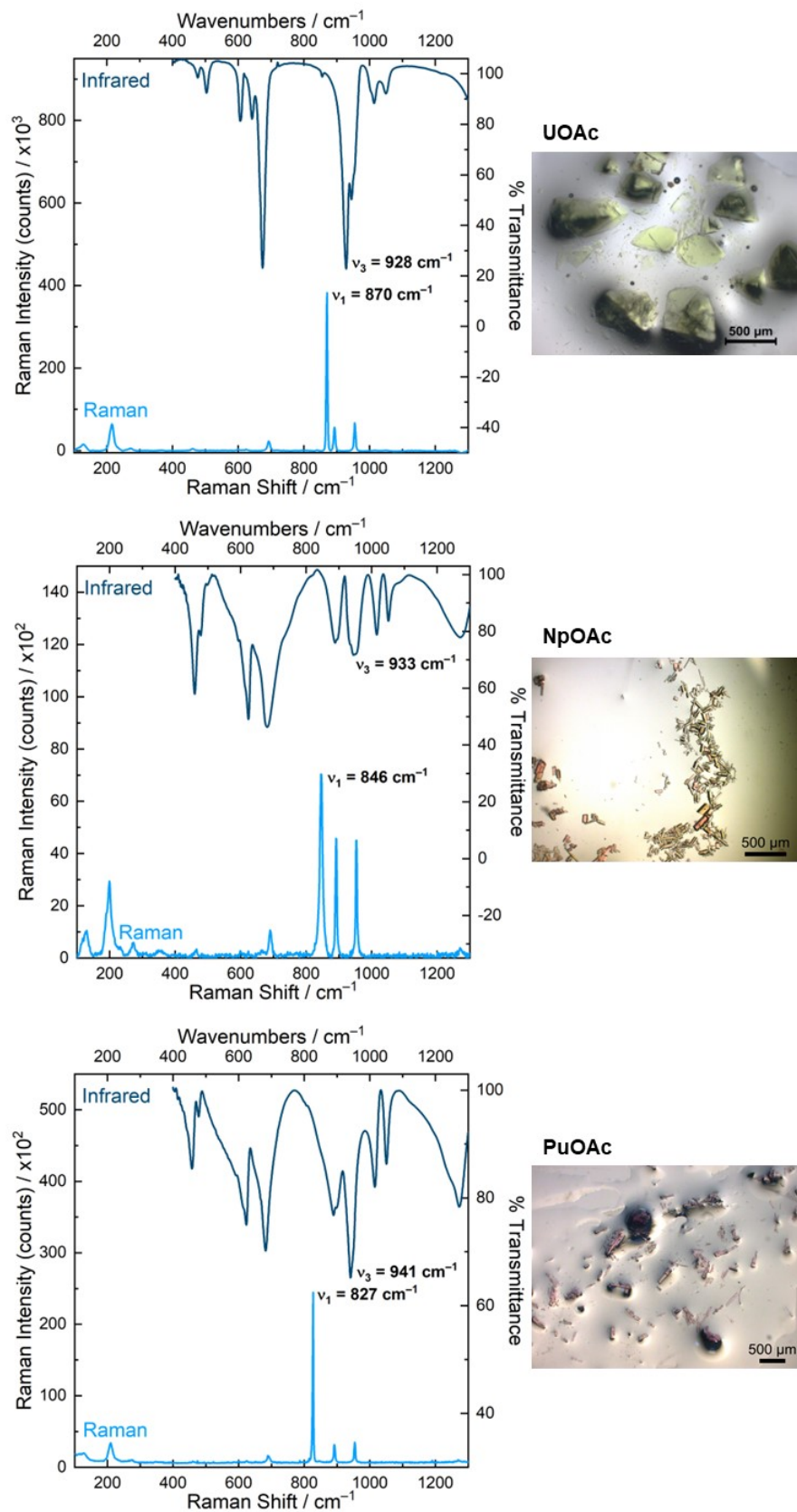
Figure 4: IR and Raman spectra of **UOAc**, **NpOAc**, and **PuOAc**.
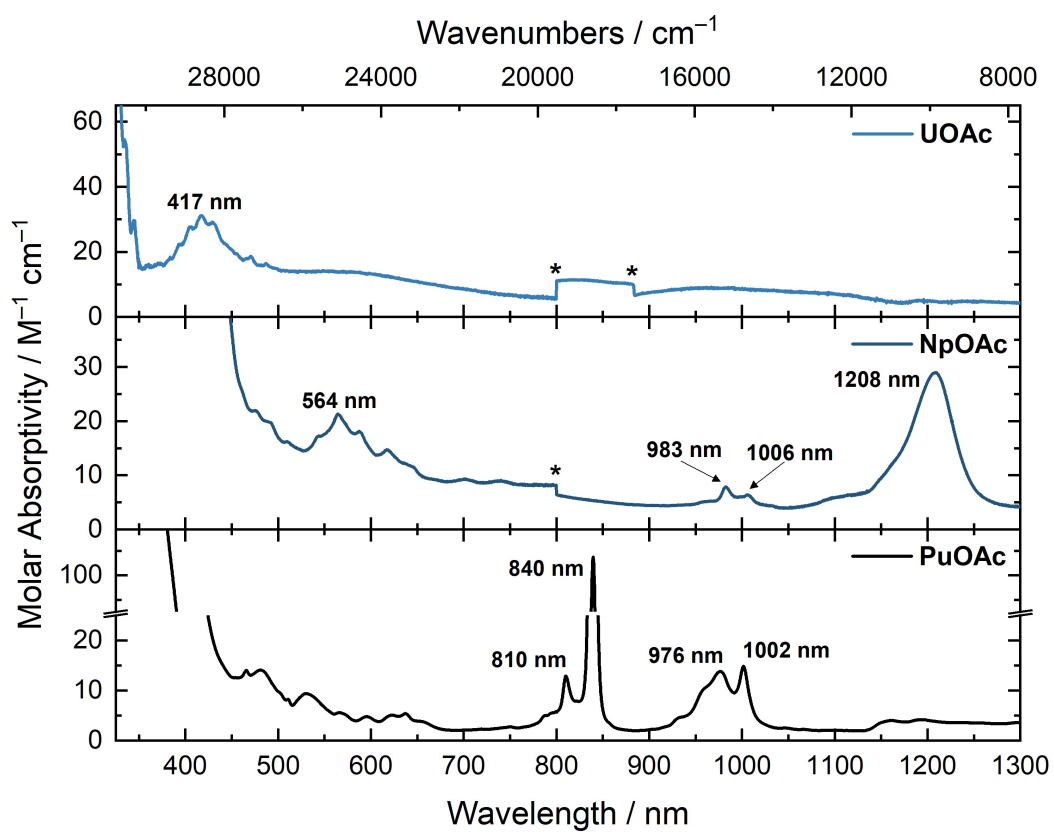
Figure 5: Optical spectra of **UOAc**, **NpOAc**, and **PuOAc** in glacial acetic acid. Asterisks indicate changes in the detector of the instrument.

and 1208 nm were measured for **NpOAc** in the visible and near-infrared (NIR) regions. Vibronic structure shown in Figure 6 can also be observed centered around the feature at 564 nm (17730 cm^{-1}), corresponding to a similar LMCT transition as that found for **UOAc** and involving CT from the oxo oxygens to Np(VI). This transition is vibronically coupled with Np–O stretching in the excited state which is reminiscent of the properties of NpO$_2^+$.[42] Vibronic structure of this type is infrequently observed for Np compounds, in part because of spectral overlap with more intense transitions often associated with equatorial ligands. However, progressions similar to that observed here have been reported for other simple coordination compounds of Np, such as [NpO$_2$(CO$_3$)$_3$]$^{-4}$, NpO$_2$(NO$_3$)$_3^-$, and NpO$_2$Cl$_4^{-2}$.[42,43] Notably, the progression measured here displays an average splitting energy of 752 cm^{-1}, which compares well to the energy of the ν_1 frequency for NpO$_2^+$ (*vide supra*). The feature at 1208 nm (ϵ = 17 M^{-1}cm^{-1}) displays a low molar extinction coefficient which is typical of *f-f* transitions for Np(VI) as they are Laporte forbidden, supporting the persistence of the Np(VI) oxidation state in solution; this feature has a similar energy and molar extinction coefficient to that of Np(VI) in HClO$_4$ (λ_{max} = 1223 nm, ϵ = 45 M^{-1}cm^{-1}).[42,44] A minor feature at 983 nm is consistent with generation of a very small amount of Np(V), approximately 2% based on the differences in molar extinction coefficients for NpO$_2^+$ and NpO$_2^{2+}$. Similarly, the optical spectrum of **PuOAc** shows several features characteristic of Pu(VI) in the near-infrared at 840, 976, and 1002 nm with molar extinction coefficients of 107, 14, and 15 M^{-1}cm^{-1}, respectively. These agree well with spectra of the PuO$_2^{2+}$ aquo ion which displays absorption maxima at 830, 950, and approx. 985 nm in HClO$_4$.[45] And, finally, contrasting with the U(VI) and Np(VI) spectra, there are no indications of vibronic structure in the Pu(VI) spectra collected.
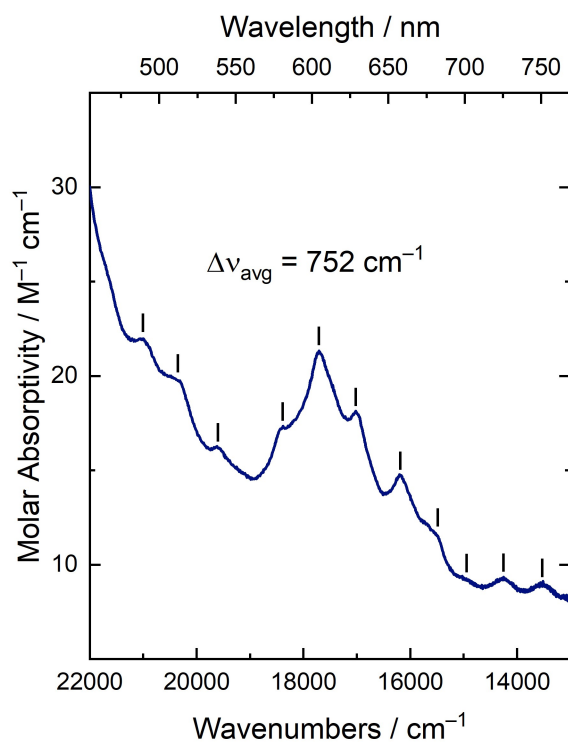
14

Figure 6: Vibronic progression observed for **NpOAc** in glacial acetic acid.

NpOAc and PuOAc as Synthons for Transuranic Coordination Compounds

With a reliable route to **NpOAc** and **PuOAc** in hand, we probed their reactivity with a diprotic Schiff base ligand for which the corresponding uranyl complex has been thoroughly characterized in prior work.[46] As shown in Figure 7, the protonolysis reactivity in this synthetic strategy relies on the two equivalents of base that are intrinsic to **NpOAc** and **PuOAc**; these acetates serve to deprotonate the organic ligand, obviating a need for exogeneous base or pre-generation of a ligand salt. Similar to uranyl acetate, both **NpOAc** and **PuOAc** are virtually insoluble in acetonitrile, but display good solubility in methanol, with their solubility increasing across the series from U to Np to Pu. Adding a solution of excess H_2L^{NM} in methanol to **NpOAc** or **PuOAc** solids resulted in an immediate color change of the solution to black in the case of neptunium and very dark green in the case of plutonium. Immediate cooling of the reaction mixture gave high yields of crystalline product (as high as

15

94% in the case of Pu), which were suitable for X-ray diffraction and spectroscopic analysis. Notably, the synthesis of the uranyl analogue proceeds under identical conditions as for Np and Pu, but a vast difference in the solubility of the product is observed. The uranyl complex precipitates almost immediately from the reaction mixture in MeOH, whereas we have found that the Np and Pu complexes must be coaxed from solution by cooling.
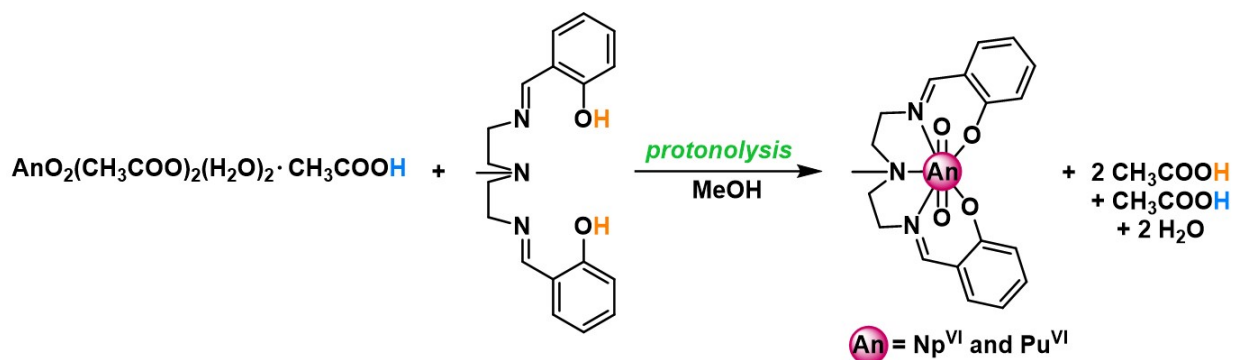

Figure 7: A balanced reaction for the synthesis of transuranic coordination compounds via protonolysis reactivity starting from **NpOAc** and **PuOAc**.

XRD analysis of single crystals obtained by cooling of the reaction solutions reveal molecular actinyl(VI) compounds in both cases as shown in Figure 8, thereby providing direct neptunium and plutonium analogues to the previously reported U(VI) compound of the same ligand.[46] Solution and refinement was straightforward for all the structures; key structural details on these complexes are given in Table 3 and details regarding the crystallography are given in the Supporting Information (pp. S92-S115 and Table ST9). In both the Np(VI) and Pu(VI) structures, the actinyl(VI) ions are coordinated to the five donor atoms of the organic ligand, with a partially occupied outer sphere co-crystallized methanol engaging in a hydrogen bond with the phenoxide O-atoms of the ligand. Bond distances for the Np and Pu complexes are consistent with retention of the +VI oxidation state upon binding to the ligand, in accord with the stability of this oxidation state in the starting materials **NpOAc** and **PuOAc**.[31,32] While the equatorial bond distances do not vary greatly across the series, the degree of ligand puckering described by the fold angle is markedly different for neptunium and plutonium compared to uranium.[47] While UO_2L^{NM} displays a fairly planar ligand

16

configuration for both of the molecules in the asymmetric unit with fold angles of 12.16(14)° and 25.35(12)° (denoted the "exo" conformation, *vide infra*), $\mathbf{NpO_2L}^{NM}$ and $\mathbf{PuO_2L}^{NM}$ feature ligands puckered at fold angles of 64.28(3)° and 61.47(2)°, respectively (denoted the "endo" conformation, *vide infra*). This is consistent with the anticipated smaller radii of the Np and Pu centers in the corresponding actinyl dications.
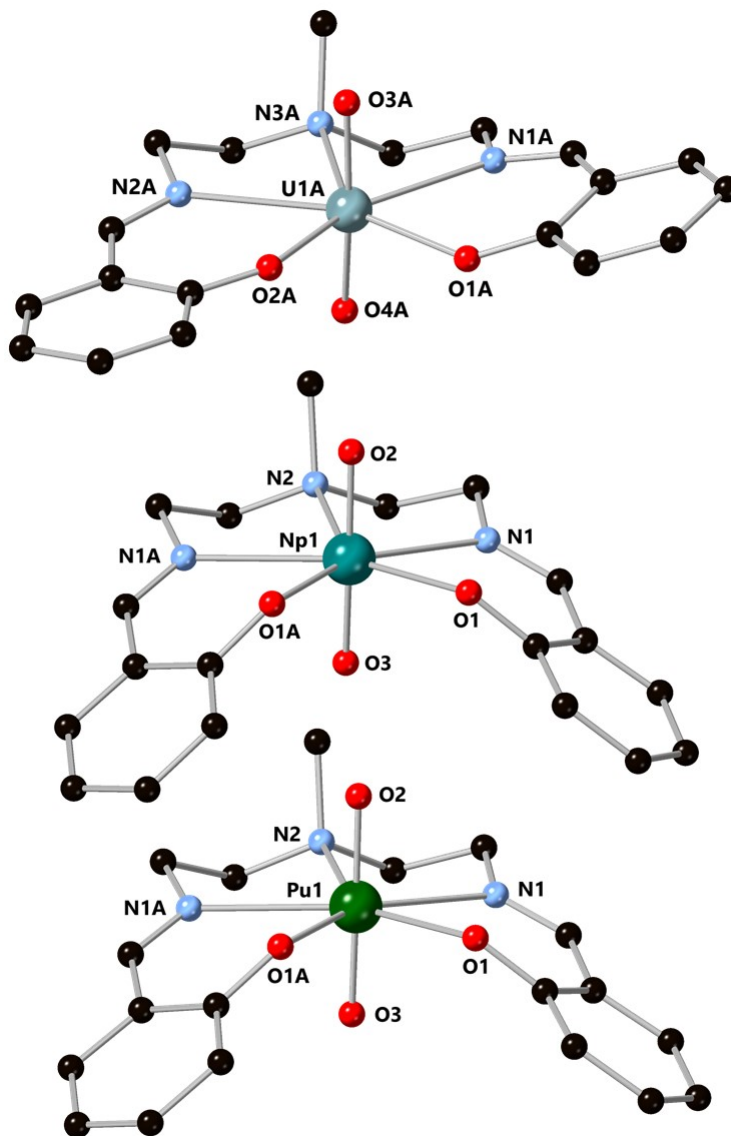

Figure 8: Ball and stick representations of $\mathbf{UO_2L}^{NM}$, $\mathbf{NpO_2L}^{NM}$, and $\mathbf{PuO_2L}^{NM}$ derived from their solid-state structures. Co-crystallized solvent molecules and all hydrogen atoms are omitted for clarity.

Table 3: Comparison of selected structural parameters from X-ray diffraction analyses of $\mathbf{AnO_2L^{NM}}$ (An = U, Np, and Pu).

	$\mathbf{UO_2L^{NM}}$	$\mathbf{NpO_2L^{NM}}$	$\mathbf{PuO_2L^{NM}}$
An-O$_{phenoxide}$ (Å)	$2.223(3)^a$	2.226(7)	2.246(4)
An-O$_{yl}$ (Å)	$1.784(3)^a$	1.743(11)	1.754(6)
An-O$_{yl}$ (Å)	$1.793(3)^a$	1.733(9)	1.742(5)
An-N$_{imine}$ (Å)	$2.579(3)^a$	2.556(8)	2.560(5)
An-N$_{amine}$ (Å)	$2.605(3)^a$	2.630(11)	2.622(6)
Ref.	Ref^{46}	This work	This work

[a] Average values are shown; value in parentheses refers to the e.s.d that is the largest for an individual entry among the independent values used to compute the average.

Vibrational and Optical Spectroscopy of the Metal-Ligand Complexes

Raman spectra of each complex are given in Figure 9 and show strong actinyl symmetric stretches at 800 cm^{-1}, 787 cm^{-1}, and 783 cm^{-1} for U, Np, and Pu, respectively, shifting 17 cm^{-1} to lower energy as the atomic number increases (see SI, Figures S12 - S17 for full spectra). Features associated with the organic ligand backbone can be observed between 300 - 1300 cm^{-1} and are in good agreement with the Raman spectrum of K$_2$L^{NM} (see SI, Figure S10 & S11). Complementary solid-state infrared spectra display asymmetric ν_3 stretches at 883, 896, and 907 cm^{-1} for U, Np, and Pu, respectively, and are notably absent in the spectrum of the ligand sans actinide (see SI, Figures S27 - S30 for full spectra and Figure S25 for the spectrum of H$_2$L^{NM}). The imine stretch shifts only slightly from 1629 cm^{-1} in the potassium salt of the ligand to 1610, 1625, and 1626 cm^{-1} for U, Np, and Pu, respectively.

Table 4: Comparison of selected Raman and IR frequencies (cm^{-1}) for $\mathbf{UO_2L^{NM}}$, $\mathbf{NpO_2L^{NM}}$, and $\mathbf{PuO_2L^{NM}}$.

	$\mathbf{UO_2L^{NM}}$	$\mathbf{NpO_2L^{NM}}$	$\mathbf{PuO_2L^{NM}}$
$\nu(\mathrm{AnO_2}^{2+})_{sym}$	800	787	783
$\nu(\mathrm{AnO_2}^{2+})_{asym}$	883	896	907
$\nu(\mathrm{C=N})$	1610	1625	1626

18
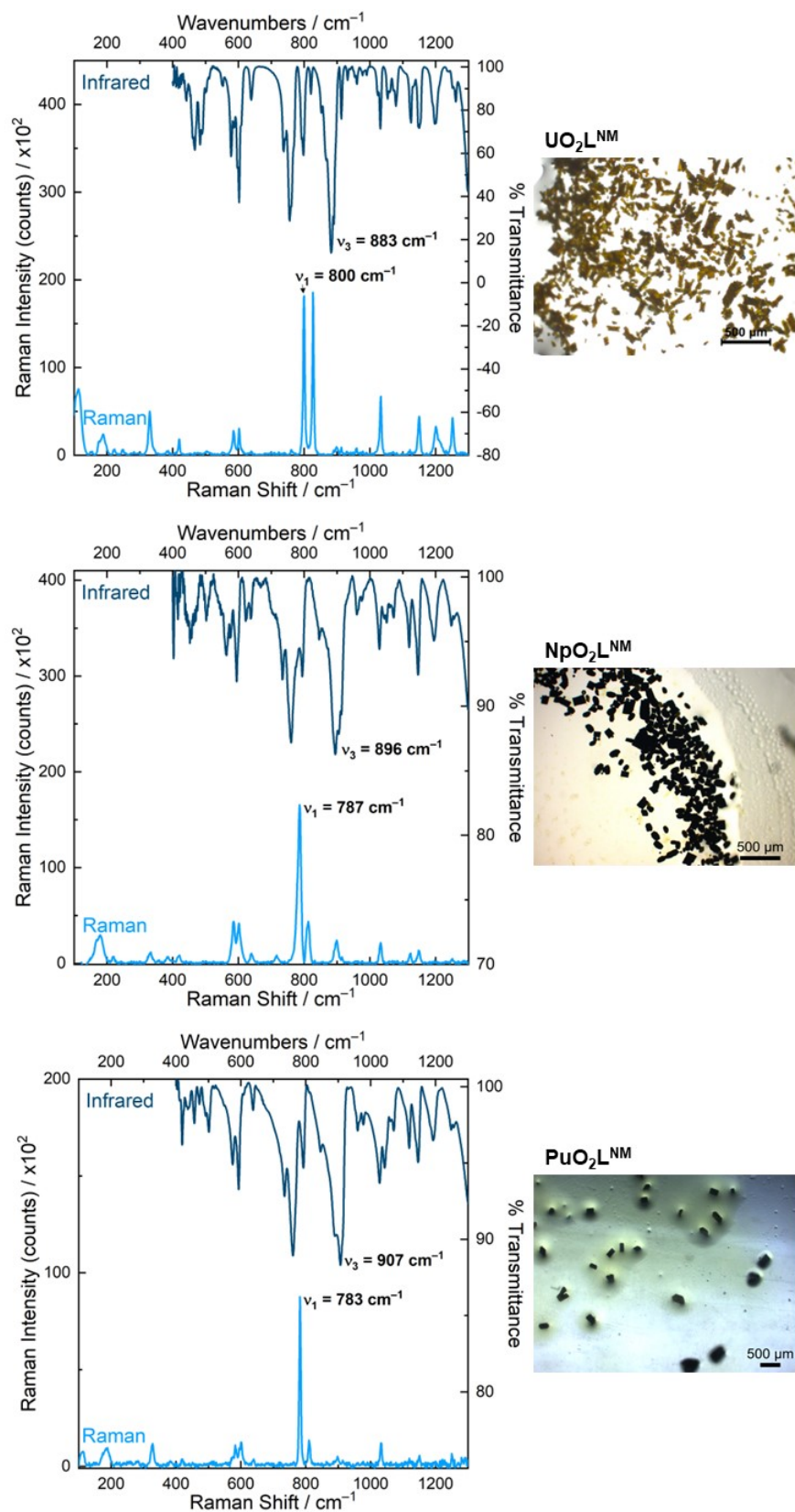
Figure 9: IR and Raman spectra of $\mathbf{UO_2L^{NM}}$, $\mathbf{NpO_2L^{NM}}$, and $\mathbf{PuO_2L^{NM}}$.

19

The solubility of all of the $\textbf{AnO}_2\textbf{L}^{NM}$ (An = U, Np, and Pu) compounds is fortuitously sufficient in acetonitrile (MeCN) to enable study of these species' solution phase properties with spectroscopy. While the UV regions of the optical spectra are dominated by intra-ligand transitions, the visible and near-infrared regions are rich in observable features associated with the actinide complexes as shown in Figure 10 (see SI Figures S37 - S42 for full spectra and molar absorptivity determinations). Consistent with its f^0 electronic configuration, the optical spectrum of the previously reported uranyl(VI) complex ($\textbf{UO}_2\textbf{L}^{NM}$) displays several maxima between 300 and 500 nm, which have been computed to arise from LMCT transitions of the equatorial ligands in similar compounds.[46,48] The optical spectra of $\textbf{NpO}_2\textbf{L}^{NM}$ and $\textbf{PuO}_2\textbf{L}^{NM}$ display absorption bands that are also likely derived from LMCT transitions at 536 and 640 nm in the case of Np and at 700 nm in the case of Pu. Notably, the NIR region of the spectrum for $\textbf{NpO}_2\textbf{L}^{NM}$ lacks any characteristic f-f transitions associated with Np(VI) or Np(V), although this is not surprising as the f-f transitions of Np(VI) species often have molar extinction coefficients of less than 100 $M^{-1}cm^{-1}$ because of their Laporte forbidden nature.[44] Nevertheless, the spectrum of $\textbf{NpO}_2\textbf{L}^{NM}$ supports the persistence the +VI oxidation state in this complex upon dissolution in MeCN, as the characteristic Np(V) absorption would likely be observable on the basis of its much higher molar extinction coefficient of approx. 500 $M^{-1}cm^{-1}$.[44] In contrast to the spectrum of $\textbf{NpO}_2\textbf{L}^{NM}$, the spectrum of $\textbf{PuO}_2\textbf{L}^{NM}$ displays characteristic features at 866 nm ($\epsilon = 327$ $M^{-1}cm^{-1}$) and 1074 ($\epsilon = 132$ $M^{-1}cm^{-1}$) which are attributable to Pu(VI).[45]
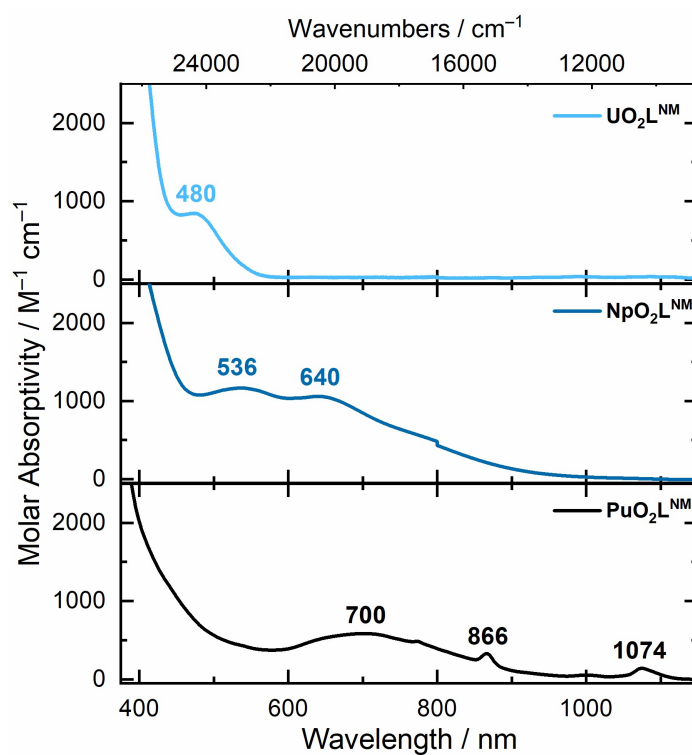
Figure 10: Optical spectra of $\mathbf{UO_2L}^{NM}$, $\mathbf{NpO_2L}^{NM}$, and $\mathbf{PuO_2L}^{NM}$ in MeCN. The discontinuity at 800 nm in the spectrum of $\mathbf{NpO_2L}^{NM}$ arises from a change in the detector in the instrument.

Computational Studies

Starting from the available X-ray crystallographic structures, molecular geometries for the $\mathbf{AnO_2L^{NM}}$ systems with An = U, Np, and Pu were optimized with scalar relativistic spin-unrestricted Kohn-Sham density functional theory (DFT) corresponding to total spins of S = 0, 1/2, and 1, respectively (full computational details are provided in the Experimental Section). The average optimized nearest-neighbor An-ligand distances in the $\mathbf{AnO_2L^{NM}}$ complexes align closely with the distances measured in the crystallographic structures, irrespective of whether the optimizations were carried out for isolated complexes (gas phase) or in the presence of a continuum solvent model representing methanol (solution phase; see SI, Tables ST3 - ST5). Superimposing the optimized and crystal structures of the complexes highlights a minor bending of the peripheral phenyl moieties upon optimization, which coincides with a slight alteration in the An-ligand distances and angles in the first coordination sphere relative to the crystal structures (see SI, Figure S43). Overall, however, it is evident from the theoretical results that the crystal structures of the $\mathbf{AnO_2L^{NM}}$ complexes are representative of the geometries that the complexes would adopt in gas phase and in solution. In other words, the conformation of the structures are not strongly influenced by crystal packing effects.

As mentioned, the XRD structure of $\mathbf{UO_2L^{NM}}$ differs from the Np and Pu analogues in that the ligand phenyl groups are stretched out in an approximately parallel fashion ("exo"). In comparison, the structures for the Np and Pu analogues have phenyl moieties that are bent toward each other ("endo"). Starting with the crystal structure of $\mathbf{NpO_2L^{NM}}$, a second molecular conformer was optimized for $\mathbf{UO_2L^{NM}}$, corresponding to a stable minimum endo structure (see SI, Figure S44). The energy difference between these conformers was calculated to be only 2.1 kJ/mol, with conformer A (exo) being lower. The conformers are effectively iso-energetic within the error limits of the DFT calculations. It is therefore plausible that even relatively minor differences in the crystal packing forces could drive crystallization towards one or the other conformer.

The chemical bonding in the $\mathbf{AnO_2L}^{NM}$ complexes was analyzed via visual and numerical assessment of the natural localized molecular orbitals (NLMOs). Representative NLMOs showing the bonding within the 'yl' unit and in the equatorial ligand plane are given in the Supporting Information (pp. S58 - S63), using the conformers corresponding to the crystal structures. Briefly, the NLMOs provide a chemically intuitive representation of the σ, π, etc., dative bonds in the complexes, as well as regular chemical bonds, lone pairs, and core-shell orbitals. Delocalization, if present, is reflected in the NLMOs. As a reminder, a dative bond leading to donation (ligand to metal, or backbonding) corresponds to a more or less pronounced delocalization of what is formally a nonbonding orbital.

The NLMOs of $\mathbf{UO_2L}^{NM}$ reveal the expected set of U–O_{yl} σ and π bonds. Close to 30% of the σ(U–O) bond orbital density is on uranium, whereas the weights are close to 21% for the π bonds. This indicates that although the U-O_{yl} interactions correspond formally to triple bonds, the bonds are polarized toward the oxygens. As a result, the calculated U–O_{yl} Wiberg bond index (WBI) is only slightly above 2 (see SI, Table ST3). Notably, in this :O≡U≡O: bond picture, even the 'rearward' oxygen lone pairs (pointing away from the U–O bonds) have almost 5% density weight on U, indicating a minor covalent interaction of these lone pairs with U, possibly involving 3-center resonance and participation of the U 6p shell as demonstrated recently for other uranium complexes with strong U–ligand bonding.[49] The 5f character on the uranium side of the σ bonds is very high (80%), and it is also high for the π bonds (61% on average). The remaining NLMOs characterize the electronic structure in the equatorial plane of uranyl where there is also clear evidence of pronounced donation, with some of the equatorial σ ligand lone pairs donating more than 10% of their density to the metal. The cumulative WBIs with the metal for the coordinating O and N atoms in the organic ligand are 0.7 and 0.3–0.4, respectively. Overall, this far exceeds the donation from equatorial halide ligands in $[UO_2X_4]^{2-}$ (X = Cl, Br) complexes as investigated recently.[50]
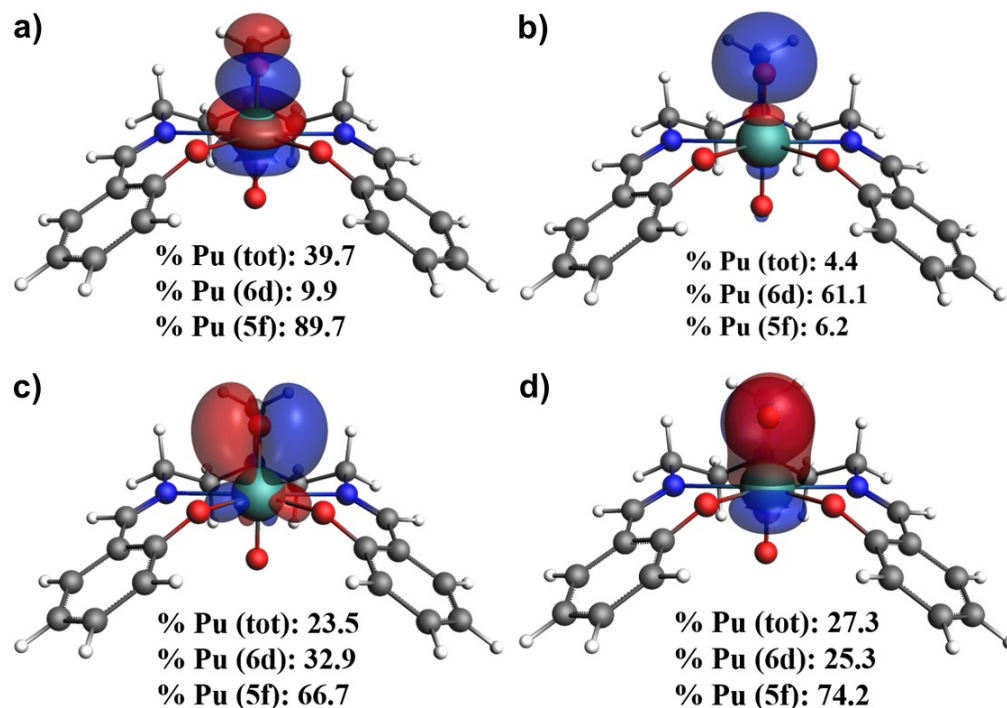
23

Figure 11: Selected natural localized molecular orbitals (NLMOs) of $\mathbf{PuO_2L}^{NM}$ showing the σ- (a and b) and π-bonding (c and d) interactions in the axial planes. Isosurfaces at ± 0.03 atomic units. The orbital density weights (%) at the metal and a breakdown of the metal contributions from the actinide 5f and 6d shells are provided beneath each NLMO/structure representation.

The bonding in $\mathbf{AnO_2L}^{NM}$ with An = Np, Pu is qualitatively the same and quantitatively very similar to the bonding in $\mathbf{UO_2L}^{NM}$, with comparable An–O_{yl} WBIs and similar An-O/N WBIs in the equatorial plane for all three actinides. The donation from equatorial ligands appears to decrease slightly from U to Np to Pu, likely as a result of the presence of one (Np) or two (Pu) electrons in non-bonding 5f orbitals, while the 'rearward' O_{yl} lone pair resonance is also slightly less pronounced for Np and Pu than it is for U. The Pu system exhibits two inequivalent σ(Pu–O_{yl}) NLMOs with an average Pu weight of 33%, indicative of 3-center-4-electron σ bonding in the 'yl' unit (Figure 11). The An–O_{yl} σ covalency appears to be somewhat more pronounced for Pu and Np than for U, which reflects the analysis of the actinyl ground state electronic structures and results from An M-edge X-ray absorption near-edge structure (XANES) spectroscopy,[51] although the trend is hardly reflected in the

24

WBIs. Based on the natural population analysis (NPA) of the calculations, the metal electronic configurations are given in Table 5 and reflect the strong donation from the ligands, in particular into the 5f shell. As a result of the donation, the calculated charges from NPA for the metal centers in the calculations with the solvent model are 1.38, 1.07, and 1.01 for U, Np, and Pu, respectively, rather than the formal +6.

Table 5: Natural charge and electronic configuration on An in the $\mathbf{AnO_2L}^{NM}$ complexes from Natural Population Analysis (NPA).

An	An charge	Electronic Configuration of An
Gas phase		
U	1.37	$7s^{0.18}5f^{2.61}6d^{1.63}7p^{0.05}$
Np	1.06	$7s^{0.19}5f^{3.94}6d^{1.59}7p^{0.05}$
Pu	1.01	$7s^{0.18}5f^{5.09}6d^{1.52}7p^{0.04}$
Solution phase		
U	1.38	$7s^{0.19}5f^{2.59}6d^{1.64}7p^{0.04}$
Np	1.07	$7s^{0.19}5f^{3.94}6d^{1.59}7p^{0.04}$
Pu	1.01	$7s^{0.19}5f^{5.07}6d^{1.53}7p^{0.04}$

A computational analysis of the vibrational modes in the $\mathbf{AnO_2L}^{NM}$ complexes was also performed. The symmetric An-O_{yl} stretching frequencies were calculated to be 825, 847, and 841 cm^{-1} for U, Np, and Pu, respectively, and the corresponding asymmetric stretching frequencies were 881, 937, and 944 cm^{-1}, respectively. These vibrational modes correspond to the exo conformer (Isomer A) for U and endo conformer for Np and Pu (Isomer B), in line with the crystallographically observed isomer for each complex. The calculated symmetric An–O_{yl} stretching frequencies for the other isomer of each complex were found to be 844, 847, and 834 cm^{-1}, with the asymmetric stretching frequencies at 918, 931, and 940 cm^{-1} for U, Np, and Pu, respectively. In the cases of Np and Pu, the $\Delta(\nu_3 - \nu_1)$ for the stretching frequencies of both conformers obtained from computation (endo: 90 and 103 cm^{-1} for Np and Pu, respectively; exo: 84 and 106 cm^{-1} for Np and Pu, respectively) compare reasonably well with experimental values (109 cm^{-1} for Np and 124 cm^{-1} for Pu). This $\Delta\nu$ value is diagnostic for U, Np, and Pu in the +VI oxidation state and the values obtained here are consistent with other An(VI) compounds for which both Raman and IR data is available.[34]

In the case of U, the calculated $\Delta(\nu_3$ - $\nu_1)$ for the crystallographically observed exo conformer is a bit underestimated in the calculation (56 cm^{-1}). The gap is higher, however, for the endo conformer (74 cm^{-1}), which agrees well with the difference observed in the experimental data (83 cm^{-1}) and suggests the existence of both isomers under experimental conditions.

To gain insight into the distinctive colors of the complexes in solution, calculations of the electronic excitation spectra were performed (see SI, Figures S51, S53, and S55). The calculated spectra have higher absolute intensities compared to the experimental data, in particular in the low-energy (long-wavelength) regions. However, deviations of calculated molar absorption coefficients by a factor of two with respect to experiments are not uncommon. The high-energy bands could be readily assigned as ligand-centered $\pi \rightarrow \pi^*$ transitions and are not considered here in detail. Corresponding assignments for the most intense transitions in the lower-energy regions of the spectra are based on natural transition orbitals (NTOs; given in the SI, pp. S65 - S73). Broadly speaking, the analyzed calculated electronic excitations are composed of mixed transitions from ligand-centered lone pairs and occupied ligand π orbitals into actinyl σ^* and π^* orbitals. Because of the equatorial donation and lack of planarity in the equatorial ligand arrangements, transitions into actinyl σ^* and π^* orbitals are not cleanly separated and the spectra do not therefore have straightforward, more detailed assignments. Separated bands in the lower-energy parts of the spectra seem to appear because of energies differences of the corresponding 'hole' orbitals, and because the pairs of actinyl π_g^* and π_u^* orbitals are not spatially degenerate in the presence of the organic ligand.

Discussion

The neutral diacetate salts **NpOAc** and **PuOAc** reported here are distinct from prior neptunyl and plutonyl acetate species; in all prior work of which we are aware, the actinyl moieties have been incorporated into anionic triacetate salts wherein the equatorial coordination

plane of the actinyl units is fully occupied by three acetate ligands. In these complexes, the formally anionic charge of the $[AnO_2(CH_3COO)_3]^-$ core is balanced by an associated alkali metal cation. These complexes do not appear broadly useful for applicatiions in synthetic chemistry, however, for three reasons: First, they display very limited solubility. Second, as additional metal cations are carried through with the actinyls, An/M metal scrambling in targeted products could be a concern. Third, and most importantly, secondary metal cations could promote actinyl reactivity. Avoiding inclusion of "surplus" cations should support clean synthetic chemistry, particularly since direct secondary metal cation coordination to actinyl units is an established strategy for An–O bond activation.[52,53] These possible complications do not appear to impact the synthesis of the $\mathbf{AnO_2L^{NM}}$ (An = Np and Pu) species report here, as shown by successful incorporation of the AnO_2^{2+} cores for both Np and Pu.

The acetate moieties in **NpOAc** and **PuOAc** appear quite able to drive protonolysis reactivity (Figure 7). Proton abstraction from the phenols in the model organic ligand used here proceeds smoothly and rapidly. These Brønsted acid/base properties of **NpOAc** and **PuOAc** enable access to the desired products in moderate to good yields, despite an apparent mismatch in the pK_a values of phenol and acetic acid (9.99 for phenol vs. 4.76 for acetic acid; values taken from measurements in aqueous media).[54,55] These values predict that acetate is not sufficiently basic to deprotonate a phenol. However, the reaction is presumably encouraged in our system by the acidification of the phenolic protons when the very Lewis acidic actinyl ions contact the donor atoms of the ligand; in this way, the intrinsic Lewis acidity of the actinyl ions works in concert with the Brønsted basicitiy of the acetate moieties to accomplish the protonolysis reactivity (The pK_a values of the $AnO_2(H_2O)_5^{2+}$ complexes are 5.3 ± 0.2, 5.1 ± 0.4, and 5.5 ± 0.5 for U, Np, and Pu, respectively.[56]) The presence of one equivalent of co-crystallized CH_3COOH in the isolated, crystalline materials used for the synthetic work does not impede the protonolysis reactivity with the incoming ligand, implying that the Lewis and Brønsted acid/base chemistry plays the key role in influencing the synthetic efficiency, rather than the associated CH_3COOH. We also note

27

that the molecular nature of the actinyl species in the complexes may also contribute to their synthetic effectiveness, in that the An centers are coordinated by both κ^2 acetates as well as aqua ligands; we anticipate that these bound waters could be readily displaced by incoming amine/imine N-atoms and/or phenol O-atoms to allow for the direct contact with the actinyl core that drives effective acidification of the phenolic protons. This situation is conceptually similar to metal-ligand (cyclo)metallation reactivity that is established to occur in organometallic chemistry by concerted deprotonation/coordination.[57]

Nearly all prior work has achieved the synthesis of coordination complexes of Np(VI) and Pu(VI) using stock solutions as sources of Np(VI) or Pu(VI), rather than employing fully characterized, stoichiometric starting materials. This is due in part to the lack of a conveient source of stabilized Np(VI) and Pu(VI); these species present rather oxidizing +VI forms, with An(VI/V) potentials under standard acidic conditions of +1.14 and +0.93 V, respectively.[26,27] In this context, the observation of acetate/aqua coordination of the $AnO_2{}^{2+}$ cores of **NpOAc** and **PuOAc** should be noted. Consider, for example, the relative symmetric ν_1 stretching frequencies for the Na^+ adduct of the Np-triacetate motif and **NpOAc**. The ν_1 values are 844 and 846 cm^{-1}, respectively, in line with the greater ligand donor strength of three formally anionic acetates in comparison to the two present in **NpOAc** that are accompanied by two bound water molecules.[58] The difference in vibrational frequency, however, between these species is only 2 cm^{-1}, in line with the observation that **NpOAc** and the analogous **PuOAc** remain virtually stable in the +VI O.S. in both the solid state and in solution. **NpOAc** and **PuOAc** reported here feature an appealing balance of stability and reactivity; the installed ligand set is sufficiently donating to enable isolation and storage of the complexes, but not so donating as to preclude reactivity with incoming ligands. Such features are common to many starting materials.

Among previously studied and isolated Np and Pu complexes, those that are perhaps the most similar to ours are $PuO_2(NO_3)_2(H_2O)_2 \cdot H_2O$ (**PuN**) from Gaunt and co-workers[59] and $NpO_2(NO_3)_2(H_2O)_2 \cdot H_2O$ (**NpN**) from Lindqvist-Reis and co-workers.[60] These complexes fea-

ture molecular actinyl species in the solid state, bridged only by H-bonding interactions. The nitrate anions are also bound in the κ^2 fashion, much like our acetates. However, the AnO_2^{2+} cores in these complexes are significantly less stabilized than those in **NpOAc** and **PuOAc**, with symmetric stretching ν_1 values in the solid state of 853 and 844 cm^{-1}, respectively. **NpOAc** and **PuOAc** feature ν_1 values of 846 and 827 cm^{-1}, with the lower energy values attributable to stabilization of the An(VI) centers from the more donating acetate ligands. Enhanced donor ability is correlated to some extent with the greater Brønsted basicity of acetate; in the studies of **PuN**, Gaunt and co-workers noted that although binding of one nitrate in $\geq$5.8 M HNO$_3$ solution was observed, the nitrate anions are not strongly bound to the Pu(VI) center. Similarly, the energetic penalty of generation of HNO$_3$ can be anticipated to be higher than generation of CH$_3$COOH, underscoring the preference for use of acetates in protonolysis reactivity as described here.

Dissolution of our diprotic ligand in methanol followed by addition of **NpOAc** and **PuOAc** results in clean generation of the desired coordination complexes, reactivity that we showcased here to demonstrate the usefulness of the acetates as synthons for Np(VI) and Pu(VI) coordination chemistry. The structural data and Raman spectra provide unambiguous evidence that the Np(VI) and Pu(VI) O.S. are retained in these complexes. We anticipate at this stage that chelation of the equatorial plane of the AnO_2^{2+} cores with our model ligand disfavors further reactivity by blocking sites in the plane that could otherwise bind protic or reducing ligands. An opportunity for future work lies in comparison of rationally designed complexes featuring other ligands that we anticipate will modulate reactivity. With the actinyl(VI) synthons in hand from this work that are useful for protonolysis reactivity, a tractable but as yet unexplored route to detailed investigation of actinyl(VI) coordination chemistry is now open.

29

Conclusion

In this work, we have reported the preparation, isolation, and solid-/solution-state spectroscopic characterization of an isomorphous family of actinyl(VI) diacetate compounds of U, Np, and Pu, as well as evidence from reaction chemistry of the usefulness of these compounds as starting materials for the preparation of transuranic coordination complexes. Spectra in the solid and solution states indicate that the actinides are in the +VI O.S. and demonstrate a degree of stabilization imparted by acetate, for example in comparison to previously studied nitrate compounds. Addition of a model diprotic ligand to **NpOAc** and **PuOAc** results in protonolysis reactivity and cleanly affords access to metal-ligand complexes; spectroscopic characterization and computational results provide support for the retention of the +VI O.S. in the products as well. As compounds with desirable solubility and reactivity properties, **NpOAc** and **PuOAc** present an attractive alternative to existing reagents for high-valent transuranic coordination chemistry. Their application in this arena is currently under investigation in our laboratories.

Experimental

Materials and Methods

Caution! ^{237}Np and ^{242}Pu are α-emitting isotopes. All experiments were conducted using strict radiological controls in purpose-built laboratories for the safe handling of α-emitting radionuclides.

All reactions were performed under ambient laboratory conditions, and all materials, with the exception of ^{237}Np and ^{242}Pu, were obtained from commercial chemical sources and used as received. KBr and KCl used for IR spectra were ground and dried for a minimum of 48 hrs at 120 °C before use. The organic ligand H_2L^{NM} was synthesized according to literature procedure.[46]

Single-Crystal X-ray Diffraction

Crystals suitable for single crystal X-ray diffraction were picked from the reaction mixture and affixed to thin glass fibers by using a quick setting epoxy. Data were collected on a Bruker APEX II diffractometer using Mo Kα radiation. All data manipulations for these structures, including data collection, integration, and scaling, were carried out using the Bruker APEX2 or APEX4 Software Suites.[61,62] Absorption corrections were applied using the program *SAD-ABS*.[63] Intrinsic phasing methods were used for the structure solutions employing *SHELXT* with subsequent refinements of the structure solution using full-matrix least-squares refinements on F^2 using *SHELXL* within the ShelXle and Olex2 GUIs.[64–67] Crystallographic data reported here have been deposited with the Cambridge Crystallographic Data Centre under accession codes 2328671 - 2328677.

The final structural model for each compound incorporated anisotropic thermal parameters for all nonhydrogen atoms; isotropic thermal parameters were used for all included hydrogen atoms. Hydrogen atoms in each complex were fixed at idealized riding model sp^2- or sp^3-hybridized positions with C–H bond lengths of 0.95 – 0.99 Å. Methyl groups were incorporated into the structural models either as sp^3-hybridized riding model groups with idealized "staggered" geometry and a C-H bond length of 0.98 Å or as idealized riding model rigid rotors (with a C–H bond length of 0.98 Å) that were allowed to rotate freely about their C–C bonds in least-squares refinement cycles. The isotropic thermal parameters of idealized hydrogen atoms in all three structures were fixed at values 1.2 (non-methyl) or 1.5 (methyl) times the equivalent isotropic thermal parameter of the carbon or oxygen atom to which they are covalently bonded.

Spectroscopy

Raman spectra were collected on single crystals harvested directly from the reaction vessels and used for single-crystal X-ray diffraction measurements. Spectra were collected using a Renishaw in-via confocal Raman microscope with circularly polarized radiation and an

excitation line of 532 and 785 nm. Solid samples were placed on a microscope slide with a concave cavity and covered with a glass coverslip affixed with epoxy. Spectra were collected using circular polarized radiation between Δv 100 and 4000 cm^{-1}. Solid-state infrared samples were collected on ground crystals (approx. 2 wt%) pressed into KBr or KCl using a Nicolet iS50 FT-IR. Data were collected over 400 - 4000 cm^{-1} with a resolution of 4 cm^{-1}. UV-vis-NIR spectra of solution phase samples were collected using a Cary 5000 UV-Vis-NIR Spectrophotometer in double beam mode with a 0.25 nm step size and 0.75 nm spectral bandwidth.

Computational Details

Kohn-Sham DFT calculations were performed using the 2023 release of the Amsterdam Density Functional (ADF) suite.[68] Restrained (only hydrogens were optimized) and full geometry optimizations and electronic structure analyses were performed using the PBE0[69] hybrid functional with 25% exact exchange in conjunction with all-electron Slater type orbital (STO) basis sets of triple-zeta doubly-polarized (TZ2P) quality for the actinides and double-zeta polarized (DZP) quality for other atoms.[70] Relativistic effects were incorporated using the scalar-relativistic zeroth-Order regular approximation (ZORA) Hamiltonian.[71] Natural localized molecular orbital (NLMO) and natural population analyses (NPA) carried out with the NBO program (version 6.0)[72] interfaced with the ADF suite. To incorporate the effects from a solvent, calculations utilized the conductor-like screening model (COSMO) with parameters for methanol, as implemented in ADF.[73]

Additional geometry optimizations followed by harmonic vibrational frequency calculations were performed to obtain vibrational modes and their frequencies as well as to confirm the complex conformers as local minima. These calculations used Gaussian 16 (G16) revision C.01[74] with the PBE0 functional, ECP60MWB pseudopotentials[75,76] and matching segmented valence basis sets[77] for the metal centers, and the Gaussian-type SVP basis[78] for the other atoms. Calculations of spectra with time-dependent DFT (TDDFT) also used

32

G16, the same functional and basis as used for the aforementioned calculations, along with the polarizable continuum model (PCM)[79] for acetonitrile as solvent. A total of 300 excited states were generated for each complex. The most intense transitions were analyzed via natural transition orbitals (NTOs).[80]

Preparation of Np(OH)$_4$

Neptunium was obtained from ANL stocks and purified through a solvent extraction process using a 20% by volume tri-n-butyl phosphate (TBP)/dodecane solution, which had been preequilibrated with 4 M HNO$_3$. The solution was oxidized to neptunium(VI) using a stream of ozone gas then contacted with an equal volume of the TBP/dodecane solvent and vigorously shaken until phase transfer of neptunium(VI) was complete. The organic phase was then contacted with a fresh aqueous phase of excess hydroxylamine HCl in 1 M HNO$_3$. The aqueous phase was then boiled to dryness and redissolved in 1 M HNO$_3$. Bulk electrolysis of this solution converted neptunium(V) to neptunium(IV), which was then precipitated with sodium hydroxide as Np(OH)$_4$ and washed several times with water until the pH was near neutral.

Preparation of Pu(OH)$_4$

Plutonium was obtained from ANL stocks and purified by passing a Pu(IV) solution in 7.5 M HNO$_3$ over an anion exchange column packed with DOWEX anion resin. The plutonium was eluted with 1 M HCl, and Pu(OH)$_4$ was precipitated by the addition of NaOH. The Pu(OH)$_4$ solids were washed with deionized water until the pH of the supernatant was near neutral.

Synthesis of UO$_2$(OAc)$_2$(H$_2$O)$_2$·HOAc (UOAc)

Tetravalent uranium was produced in nitric acid by electrolysis at a platinum electrode and U(OH)$_4$ was precipitated by sodium hydroxide. The U(OH)$_4$ solids were taken up in glacial acetic acid and oxidized using a steam of air overnight yielding a pale yellow precipitate. The solids were isolated by centrifugation in a yield of 50%. Additional material of the same composition was isolated from the evaporation of the supernatant, for a total yield of 80%.

Synthesis of NpO$_2$(OAc)$_2$(H$_2$O)$_2$·HOAc (NpOAc)

The Np(OH)$_4$ solids were taken up in glacial acetic acid and oxidized using a stream of ozone gas while stirring for 1 hour. Concentration of this solution resulted in the formation of green solids, which were redissolved in minimal glacial acetic acid (approx. 1 mL). Oxidation of the solids by a stream of ozone with stirring overnight yielded a magenta precipitate in high yields (80%).

Synthesis of PuO$_2$(OAc)$_2$(H$_2$O)$_2$·HOAc (PuOAc)

The Pu(OH)$_4$ solids were taken up in glacial acetic acid with a concentration of approximately 10 mg/mL and oxidized using a steam of ozone gas for two days. During this time, the product formed as a greenish-red precipitate in a 59% yield.

Synthesis of AnO$_2$L^{NM} complexes (An = Np and Pu)

The excess organic ligand H$_2$L^{NM} was dissolved in a minimum volume of methanol and added to the respective molecular actinyl diacetate solids (**NpOAc** or **PuOAc**). Upon addition of ligand, the solution became very dark in both cases. Cooling of each reaction mixture overnight gave rise to dark crystals in both cases with yields of 82% in the case of **NpO$_2$L^{NM}** and 94% in the case of **PuO$_2$L^{NM}**.

Acknowledgement

Supporting Information Available

The following files are available free of charge:

Raman, infreared, and optical spectra, detailed information about X-ray crystallographic data, and Cartesian coordinates of optimized geometries used for computational investigations (PDF)

Cartesion coordinates for structures from XRD (XYZ)

Computational coordinates (XYZ)

References

(1) Abe, K.; Matsufuji, K.; Ohba, M.; Ōkawa, H. Site Specificity of Metal Ions in Heterodinuclear Complexes Derived from an "End-Off" Compartmental Ligand. *Inorg. Chem.*

35

2002, *41*, 4461–4467.

(2) Golwankar, R. R.; Kumar, A.; Day, V. W.; Blakemore, J. D. Revealing the Influence of Diverse Secondary Metal Cations on Redox-Active Palladium Complexes. *Chem. Eur. J.* **2022**, *28*, e202200344.

(3) Inomata, Y.; Takei, T.; Howell, F. Synthesis and crystal structure of lanthanide metal complexes with N,N-bis(2-hydroxyethyl)glycine. *Inorg. Chim. Acta* **2001**, *318*, 201–206.

(4) Van Staveren, C. J.; Van Eerden, J.; Van Veggel, F. C. J. M.; Harkema, S.; Reinhoudt, D. N. Cocomplexation of neutral guests and electrophilic metal cations in synthetic macrocyclic hosts. *J. Am. Chem. Soc.* **1988**, *110*, 4994–5008.

(5) Avens, L. R.; Bott, S. G.; Clark, D. L.; Sattelberger, A. P.; Watkin, J. G.; Zwick, B. A Convenient Entry into Trivalent Actinide Chemistry: Synthesis and Characerization of $AnI_3(THF)_4$ and $An[N(SiMe_3)_2]_3$ (An = U, Np, Pu). *Inorg. Chem.* **1994**, *33*, 2248–2256.

(6) Jones, M. B.; J., G. A. Recent Developments in Synthesis and Structural Chemistry of Nonaqueous Actinide Complexes. *Chem. Rev.* **2013**, *113*, 1137–1198.

(7) Arnold, P. L.; Dutkiewicz, M. S.; Walter, O. Organometallic Neptunium Chemistry. *Chem. Rev.* **2017**, *117*, 11460–11475.

(8) Reilly, S. D.; Brown, J. L.; Scott, B. L.; Gaunt, A. J. Synthesis and characterization of $NpCl_4(DME)_2$ and $PuCl_4(DME)_2$ neutral transuranic An(IV) starting materials. *Dalton Trans.* **2014**, *43*, 1498–1501.

(9) Goodwin, C. A. P.; Janicke, M. T.; Scott, B. L.; Gaunt, A. J. $[AnI_3(THF)_4]$ (An = Np, Pu) Preparation Bypassing An^0 Metal Precursors: Access to Np^{3+}/Pu^{3+} Nonaqueous and Organometallic Complexes. *J. Am. Chem. Soc.* **2021**, *143*, 20680–20696.

(10) Schnaars, D. D.; Wilson, R. E. Synthesis, Structure, and Vibrational Properties of $[Ph_4P]_2NpO_2Cl_4$ and $[Ph_4P]_2PuO_2Cl_4$ Complexes. *Inorg. Chem.* **2018**, *57*, 3008–3016.

36

(11) Copping, R.; Mougel, V.; Petit, S.; Auwer, C. D.; Moisy, P.; Mazzanti, M. A versatile precursor for non-aqueous neptunyl(v) chemistry. *Chem. Commun.* **2011**, *47*, 5497–5499.

(12) Klamm, B. E.; Windorff, C. J.; Celis-Barros, C.; Beltran-Leiva, M. J.; Sperling, J. M.; Albrecht-Schönzart, T. E. Exploring the Oxidation States of Neptunium with Schiff Base Coordination Complexes. *Inorg. Chem.* **2020**, *59*, 18035–18047.

(13) Zachariasen, W. H. Crystal chemical studies of the 5f-series of elements. XII. New compounds representing known structure types. *Acta Cryst.* **1949**, *2*, 388–390.

(14) Kornyakov, I. V.; Kalashnikova, S. A.; Gurzhiy, V. V.; Britvin, S. N.; Belova, E. V.; Krivovichev, S. V. Synthesis, characterization and morphotropic transitions in a family of M[(UO$_2$)(CH$_3$COO)$_3$](H$_2$O)n (M=Na, K, Rb, Cs; n=0–1.0) compounds. *Zeitschrift für Kristallographie - Crystalline Materials* **2020**, *235*, 95–103.

(15) Duffield, R. B. Process for Separation of Heavy Metals. US Patent 2832793, 1958.

(16) Choppin, G. R.; Rao, L. F. Complexation of Pentavalent and Hexavalent Actinides by Fluoride. *Radiochim. Acta* **1984**, *37*, 143–146.

(17) Howatson, J.; Grev, D.; Morosin, B. Crystal and molecular structure of uranyl acetate dihydrate. *J. Inorg. and Nucl. Chem.* **1975**, *37*, 1933–1935.

(18) Grigor'ev, M. S.; Antipin, M. Y.; Krot, N. N. Behavior of Anhydrous Uranyl Acetate at Heating in CH$_3$CN. Crystal Structures of New Uranyl Acetates. *Radiochemistry* **2004**, *46*, 224–231.

(19) Grigor'ev, M. S.; Antipin, M. Y.; Krot, N. N. Diacetatodiaquadioxouranium(VI) acetic acid disolvate. *Acta Cryst., Sect. E* **2005**, *61*, 2078–2079.

(20) Forni, L.; Bahnemann, D.; Hart, E. J. Mechanism of the Hydrozide Ion Initiated Decomposition of Ozone in Aqueous Solution. *J. Phys. Chem* **1982**, *86*, 255–259.

(21) Sehested, K.; Holcman, J.; Bjergbakke, E.; Hart, E. J. Ozone Decomposition in Aqueous Acetate Solutions. *J. Phys. Chem.* **1987**, *91*, 2359–2361.

(22) Almond, P. M.; Skanthakumar, S.; Soderholm, L.; Burns, P. C. Cation-Cation Interactions and Antiferromagnetism in $Na[Np(V)O_2(OH)_2]$: Synthesis, Structure, and Magnetic Properties. *Chem. Mat.* **2007**, *19*, 280–285.

(23) Vlaisavljevich, B.; Miró, P.; Ma, D.; Sigmon, G. E.; Burns, P. C.; Cramer, C. J.; Gagliardi, L. Synthesis and Characterization of the First 2-D Neptunyl Structure Stabilized by Side-on Cation–Cation Interactions. *Chem. Eur. J.* **2013**, *19*, 2937–2941.

(24) Wilson, R. E.; Stegman, S.; Tarlton, M. L. Reactions of Neptunium(V) in Alkali-Metal Hydroxides. *Inorg. Chem.* **2021**, *60*, 17480–17486.

(25) Fellhauer, D.; Lee, J.-Y.; DiBlasi, N. A.; Walter, O.; Gaona, X.; Schild, D.; Altmaier, M. Crystal Structure and Stability in Aqueous Solutions of $Na_{0.5}[NpO_2(OH)_{1.5}] \cdot 0.5H_2O$ and $Na[NpO_2(OH)_2]$. *J. Am. Chem. Soc.* **2022**, *144*, 9217–9221.

(26) Burney, G. A.; Harbour, R. M. *Radiochemistry of Neptunium*; United States Atomic Energy Commission: Aiken, South Carolina, 1974.

(27) Coleman, G. H. *The Radiochemistry of Plutonium*; United States Atomic Energy Commission: Livermore, California, 1965.

(28) Magnusson, L. B.; LaChapelle, T. J. The First Isolation of Element 93 in Pure Compounds and a Determination of the Half-life of $_{93}Np^{237}$. *J. Am. Chem. Soc.* **1948**, *70*, 3534–3538.

(29) Bessonov, A. A.; Grigor'ev, M. S.; Afonas'eva, T. V.; Krot, N. N. Simple Neptunium(V) Acetates. *Radiokhimiya* **1988**, *31*, 33–37.

(30) Bratsch, S. G. Standard Electrode Potentials and Temperature Coefficients in Water at 298.15 K. *Journal of Physical and Chemical Reference Data* **1989**, *18*, 1–21.

(31) Gilson, S. E.; Burns, P. C. The crystal and coordination chemistry of neptunium in all its oxidation states: An expanded structural hierarchy of neptunium compounds. *Coord. Chem. Rev.* **2021**, *445*, 213994.

(32) Serezhkin, V. N.; Savchenkov, A. V.; Sidorenko, G. V.; Serezhkina, L. B. Actinide Contraction in Oxygen-Containing An(VI) Compounds. *Radiochemistry* **2019**, *61*, 408–419.

(33) Cowie, B. E.; Purkis, J. M.; Austin, J.; Love, J. B.; Arnold, P. L. Thermal and Photochemical Reduction and Functionalization Chemistry of the Uranyl Dication, $[U^{VI}O_2]^{2+}$. *Chem. Rev.* **2019**, *119*, 10595–10637.

(34) Autillo, M.; Wilson, R. E.; Vasiliu, M.; de Melo, G. F.; Dixon, D. A. Periodic Trends within Actinyl(VI) Nitrates and Their Structures, Vibrational Spectra, and Electronic Properties. *Inorg. Chem.* **2022**, *61*, 15607–15618.

(35) Denning, R. G. *Complexes, Clusters and Crystal Chemistry*; Springer, 1992; Chapter Electronic structure and bonding in actinyl ions, pp 215–276.

(36) Denning, R. G. Electronic Structure and Bonding in Actinyl Ions and their Analogs. *J. Phys. Chem. A* **2007**, *111*, 4125–4143.

(37) Hay, P. J.; Martin, R. L.; Schreckenbach, G. Theoretical Studies of the Properties and Solution Chemistry of AnO_2^{2+} and AnO_2^+ Aquo Complexes for An = U, Np, and Pu. *J. Phys. Chem. A* **2000**, *104*, 6259–6270.

(38) Fletcher, P. D. I.; Haswell, S. J.; Zhang, X. Monitoring of chemical reactions within microreactors using an inverted Raman microscopic spectrometer. *Electrophor.* **2003**, *24*, 3239–3245.

(39) Lewis, I. R.; Edwards, E. G. M. *Handbook of Raman Spectroscopy - From the Research Laboratory to the Process Line*; Marcel Dekker: New York, 2001.

(40) Bard, A. J.; Parsons, R.; Jordan, J. *Standard Potentials in Aqueous Solution*; CRC Press: New York, New York, 1985.

(41) Bell, J. T.; Biggers, R. E. The Absorption Spectrum of the Uranyl Ion in Perchlorate Media. *J. Mol. Spectrosc.* **1965**, *18*, 247–275.

(42) Denning, R. G.; Norris, J. O. W. The electronic structure of actinyl ions V. f-f transitions in $[NpO_2Cl_4]^{2-}$ and $[NpO_2(NO_3)_3]^-$. *Mol. Phys.* **1982**, 287–323.

(43) Ikeda-Ohno, A.; Tsushima, S.; Takao, K.; Rossberg, A.; Funke, H.; Scheinost, A. C.; Bernhard, G.; Yaita, T.; Hennig, C. Neptunium Carbonato Complexes in Aqueous Solution: An Electrochemical, Spectroscopic, and Quantum Chemical Study. *Inorg. Chem.* **2009**, *48*, 11779–11787.

(44) Hagan, P. G.; Cleveland, J. M. The Absorption Spectra of Neptunium Ions in Perchloric Acid Solution. *J. Inorg. Nucl. Chem.* **1966**, *28*, 2905–2090.

(45) Cohen, D. The Absorption Spectra of Plutonium Ions in Perchloric Acid Solutions. *J. Inorg. Nucl. Chem.* **1961**, *18*, 211–218.

(46) Golwankar, R. R.; Makos, M. Z.; Cajiao, N.; Neidig, M. L.; Oliver, A. G.; Day, C. S.; Day, V. W.; Glezakou, V.-A.; Blakemore, J. D. Electrochemical Activation and Functionalization of the Uranyl Ion. *ChemRxiv* **2023**,

(47) Calligaris, M.; Nardin, G.; Randaccio, L. Structural aspects of metal complexes with some tetradentate Schiff bases. *Coord. Chem. Rev.* **1972**, *7*, 385–403.

(48) Azam, M.; Al-Resayes, S. I.; Velmurugan, G.; Venuvanalingam, P.; Wagler, J.; Kroke, E. Novel uranyl(VI) complexes incorporating propylene-bridged salen-type N_2O_2-ligands: a structural and computational approach. *Dalton Trans.* **2015**, *44*, 568–577.

(49) Motta, L. C.; Autschbach, J. Actinide inverse trans influence versus cooperative pushing from below and multi-center bonding. *Nat. Commun.* **2023**, *14*, 4307–4317.
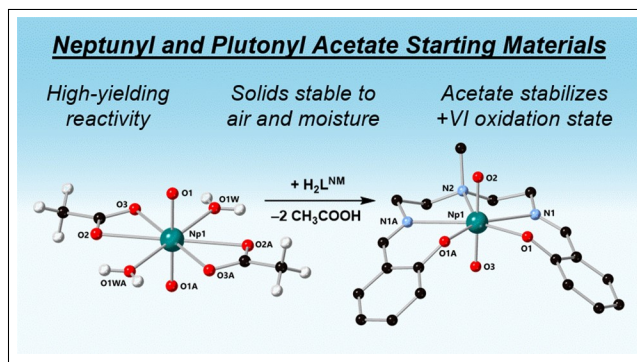
(50) Sergentu, D.-C.; Gendron, F.; Walter, E. D.; Park, S.; Capan, C.; Surbella III, R. G.; Soderquist, C. Z.; Hall, G. B.; Sinkov, S. I.; Autschbach, J.; Cho, H. Equatorial Electronic Structure in the Uranyl Ion: $Cs_2UO_2Cl_4$ and $Cs_2UO_2Br_4$. *Inorg. Chem.* **2022**, *61*, 3821–3831.

(51) Sergentu, D.-C.; Duignan, T. J.; Autschbach, J. Ab Initio Study of Covalency in the Ground versus Core-Excited States and X-ray Absorption Spectra of Actinide Complexes. *J. Phys. Chem. Lett.* **2018**, *9*, 5583–5591.

(52) Arnold, P. L.; Pecharman, A. G.; Hollis, E.; Yahia, A.; Maron, L.; Parsons, S.; Love, J. B. Uranyl oxo activation and functionalization by metal cation coordination. *Nature Chem.* **2010**, *2*, 1056–1061.

(53) Camp, C.; Chatelain, L.; Mougel, V.; Pecaut, J.; Mazzanti, M. Ferrocene-Based Tetradentate Schiff Bases as Supporting Ligands in Uranium Chemistry. *Inorg. Chem.* **2015**, *54*, 5772–5783.

(54) *PubChem Compound Summary for CID 996, Phenol*; National Center for Biotechnology Information, 2024.

(55) *PubChem Compound Summary for CID 176, Acetic Acid*; National Center for Biotechnology Information, 2024.

(56) Palmer, D.; Guillaumont, R.; Fanghaenel, T.; Neck, V.; Fuger, J.; Grenthe, I.; Rand, M. *Update on the Chemical Thermodynamics of Uranium, Neptunium, Plutonium, Americium, and Technitium*; Elsevier, 2003.

(57) Davies, D. L.; Al-Duaij, O.; Fawcett, J.; Giardiello, M.; Hilton, S. T.; Russell, D. R. Room-temperature cyclometallation of amines, imines and oxazolines with $[MCl_2Cp^*]_2$ (M = Rh, Ir) and $[RuCl_2(p\text{-cymene})]_2$. *Dalton Trans.* **2003**, 4132–4138.

41

(58) Jones, L. H. Infrared Spectra and Structure of the Crystalline Sodium Acetate Complexes of U(VI), Np(VI), Pu(VI), and Am(VI). A Comparison of Metal-Oxygen Bond Distance and Bond Force Constant in this Series. *J. Chem. Phys.* **1954**, *23*, 2105–2107.

(59) Gaunt, A. J.; May, I.; Neu, M. P.; Reilly, S. D.; Scott, B. L. Structural and Spectroscopic Characterization of Plutonyl(VI) Nitrate under Acidic Conditions. *Inorg. Chem.* **2011**, *50*, 4244–4246.

(60) Lindqvist-Reis, P.; Apostolidis, C.; Walter, O.; Marsac, R.; Banik, N. L.; Skripkin, M. Y.; Rothe, J.; Morgenstern, A. Structure and spectroscopy of hydrated neptunyl(vi) nitrate complexes. *Dalton Trans.* **2013**, *42*, 15275–15279.

(61) *SAINT, Ver 8.34A*; Bruker Analytical X-ray Systems: Madison, WI, 2014.

(62) *APEX2, Version 2 User Manual, M86-E01078*; Bruker Analytical X-ray Systems: Madison, WI, 2006.

(63) Sheldrick, G. M.; Howard, G. SADABS. *Coord. Chem. Rev.* **2003**, *Version 2.10*, University of Gottingen.

(64) Sheldrick, G. M. SHELXT - Integrated Space-Group and Crystal-Structure Determination. *Acta Cryst. A.* **2015**, *71*, 3–8.

(65) Sheldrick, G. M. Crystal structure refinement with SHELXL. *Acta Cryst., Sect. C* **2015**, *71*, 3–8.

(66) Hubschle, C. B.; Sheldrick, G. M.; Dittrich, B. ShelXle: a Qt Graphical User Interface for SHELXL. *J. Appl. Cryst.* **2011**, *44*, 1281–1284.

(67) Dolomanov, O. V.; Bourhis, L. J.; Gildea, R. J.; Howard, J. A.; Puschmann, H. OLEX2: a complete structure solution, refinement, and analysis program. *J. Appl. Crystallogr.* **2009**, *42*, 339–341.

(68) Baerends, E. J. et al. ADF2023, SCM, Theoretical Chemistry, Vrije Universiteit, Amsterdam, The Netherlands, https://www.scm.com.

(69) Adamo, C.; Barone, V. Toward reliable density functional methods without adjustable parameters: The PBE0 model. *J. Chem. Phys.* **1999**, *110*, 6158–6170.

(70) van Lenthe, E.; Baerends, E. J. Optimized Slater-type basis sets for the elements 1-118. *J. Comput. Chem.* **2003**, *24*, 1142–1156.

(71) van Lenthe, E.; Baerends, E. J.; Snijders, J. G. Relativistic regular two-component Hamiltonians. *J. Chem. Phys.* **1993**, *99*, 4597–4610.

(72) Glendening, E. D.; Landis, C. R.; Weinhold, F. Natural bond orbital methods. *Wiley Interdiscip. Rev.: Comput. Mol. Sci.* **2012**, *2*, 1–42.

(73) Pye, C. C.; Ziegler, T. An implementation of the conductor-like screening model of solvation within the Amsterdam density functional package. *Theor. Chem. Acc.* **1999**, *101*, 396–408.

(74) Frisch, M. J. et al. Gaussian 16 Revision C.01. Gaussian, Inc., Wallingford CT, 2016. URL: www.gaussian.com.

(75) Andrae, D.; Haeussermann, U.; Dolg, M.; Stoll, H.; Preu, H. Energy-adjusted ab initio pseudopotentials for the second and third row transition elements. *Theor. Chim. Acta* **1990**, *77*, 123–141.

(76) Cao, X.; Dolg, M. Relativistic energy–consistent ab initio pseudopotentials as tools for quantum chemical investigations of actinide systems. *Coord. Chem. Rev.* **2006**, *250*, 900–910.

(77) Martin, J. M. L.; Sundermann, A. Correlation consistent valence basis sets for use with the Stuttgart–Dresden–Bonn relativistic effective core potentials: The atoms Ga–Kr and In–Xe. *J. Chem. Phys.* **2001**, *114*, 3408–3420.

(78) Schäfer, A.; Horn, H.; Ahlrichs, R. Fully optimized contracted Gaussian basis sets for atoms Li to Kr. *J. Chem. Phys.* **1992**, *97*, 2571–2577.

(79) Tomasi, J.; Persico, M. Molecular interactions in solution: An overview of methods based on continuous distributions of the solvent. *Chem. Rev.* **1994**, *94*, 2027–2094.

(80) Martin, R. L. Natural transition orbitals. *J. Chem. Phys.* **2003**, *118*, 4775–4777.

TOC Graphic

Neptunyl and Plutonyl Acetate Starting Materials

High-yielding reactivity   *Solids stable to air and moisture*   *Acetate stabilizes +VI oxidation state*

$+ H_2L^{NM}$
$-2 CH_3COOH$

NpO_2^{2+} and PuO_2^{2+} diacetate complexes have been prepared and shown to be useful for preparation of well-defined An(VI) coordination complexes via protonolysis reactivity. Joint computational work supports stabilization of the +VI oxidation state, confirming that the new acetate precursors represent useful entry points for transuranium coordination chemistry.

45